Mean-field approach to Rydberg facilitation in a gas of atoms at high and low temperatures

Daniel Brady ⦿ and Michael Fleischhauer ⦿

Department of Physics and Research Center OPTIMAS, University of Kaiserslautern-Landau, D-67663 Kaiserslautern, Germany

The excitation spread caused by Rydberg facilitation in a gas of laser-driven atoms is an interesting model system for studying epidemic dynamics. We derive a mean-field approach to describe this facilitation process in the limits of high and low temperatures, which takes into account Rydberg blockade and the network character of excitation spreading in a low-temperature gas. As opposed to previous mean-field models, our approach accurately predicts all stages of the facilitation dynamics from the initial fast epidemic growth, an extended saturation period, to the final relaxation phase.

I. INTRODUCTION

Rydberg atoms have gained a lot of interest in the last few decades due to their strongly exaggerated properties. In particular, they have very long life times and strong interactions over distances covering several m [1]. These features allow Rydberg systems to be especially useful in a multitude of applications such as quantum information processing [2–6] or the study of many-body spin physics [7–14].

One interesting process in many-body Rydberg systems is Rydberg facilitation, which has been used to study dissipative or kinetically constrained spin systems [15,16], transport and localization phenomena in disordered systems [17], or self-organized criticality [18,19].

In this type of many-body system, atoms are coupled off-resonantly to a Rydberg state. As a result of the Rydberg dipole interaction, however, atoms near an already excited Rydberg atom can be excited resonantly. Thus an initial seed excitation can lead to a cascade of excitations. It has been shown experimentally that this type of system bears close similarities to epidemic dynamics [20].

The most simple description of epidemic-type systems is given by susceptible-infected-susceptible (SIS) models. Here, each individual has two internal states, susceptible (S) or infected (I). Susceptible individuals are infected with the rate κ and infected individuals return to the susceptible state with the rate γ [21–23].

Under the assumption of homogeneous mixing, where all individuals interact with each other completely at random, all information about the epidemic dynamics is contained in the total fractions ρ^ν in the susceptible ($\nu = S$) and infected state ($\nu = I$), which obey the simple homogeneous mean-field equations given by [24]

$$\frac{\mathrm{d}}{\mathrm{d}t}\rho^I = \kappa \rho^I \rho^S - \gamma \rho^I, \tag{1a}$$

$$\frac{\mathrm{d}}{\mathrm{d}t}\rho^S = -\kappa \rho^I \rho^S + \gamma \rho^I. \tag{1b}$$

This system features an absorbing-state phase transition between two dynamical phases, namely, an absorbing phase in which all infections die out, and an active phase where, in the

thermodynamic limit, infections last forever. A suitable order parameter to distinguish these phases is the steady-state active (infected) density ρ^I_{ss}. From Eq. (1a) one recognizes that this phase transition occurs when

$$\rho^S \kappa = \gamma. \tag{2}$$

In addition to the SIS model, which describes diseases where repeat infections are common (predominantly sexually transmitted diseases) the susceptible-infected-recovered (SIR) model can be used to describe diseases which feature life-long immunity in individuals following an infection, such as measles or whooping cough [25]. The SIR model features a recovered state R, with the respective population as ρ^R. The dynamics are given by [26–28]

$$\frac{\mathrm{d}}{\mathrm{d}t}\rho^S = -\kappa \rho^I \rho^S, \tag{3a}$$

$$\frac{\mathrm{d}}{\mathrm{d}t}\rho^I = \kappa \rho^I \rho^S - \gamma \rho^I, \tag{3b}$$

$$\frac{\mathrm{d}}{\mathrm{d}t}\rho^R = \gamma \rho^I. \tag{3c}$$

The dynamics of both SIS and SIR models are well understood in the homogeneous mean-field regime. While the homogeneous mixing assumption is well justified in systems where the infection spreading occurs on a regular lattice in high spatial dimensions, it fails in many relevant cases, for example, if the the SIS-SIR dynamics take place on real-life networks. For such network systems, including, e.g., random Erdős-Rényi (ER) [29] and scale-free (SF) networks [30], a large body of more sophisticated approximation methods have been developed [31–33], but many questions remain unsolved. Here, Rydberg atoms provide a platform to experimentally investigate the epidemic dynamics on a variety of complex networks, which can, e.g., be engineered by the use of tweezer arrays [10]. Moreover, in a gas of atoms contained in some macroscopic trapping potential one can investigate the transition between a random ER network at very low temperatures, where the motion of atoms on the relevant timescales of the facilitation process can be ignored, to the homogeneous
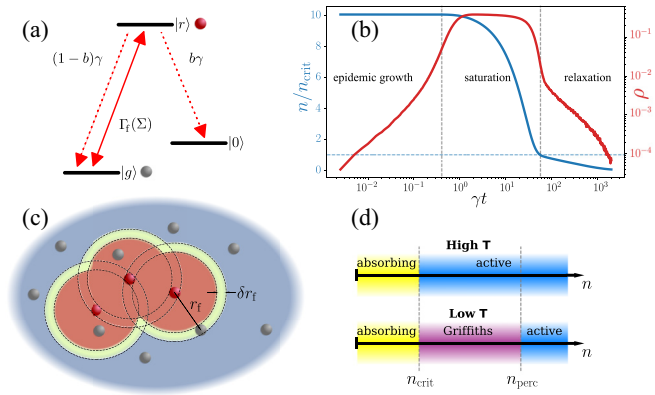
FIG. 1. (a) Level scheme of internal atomic states with ground $|g\rangle$ (susceptible) state, Rydberg $|r\rangle$ (infected) state, and inert $|0\rangle$ (recovered) state. An external laser drives the transition between $|g\rangle$ and $|r\rangle$ and spontaneous decay occurs from $|r\rangle$ to either $|g\rangle$ or $|0\rangle$, modulated by branching parameter $b \in [0, 1]$. (b) Monte Carlo data of the Rydberg density ρ (red) and total active density n (in states $|g\rangle$ and $|r\rangle$) (blue) over time, with $b = 0.3$ and initial condition $\rho(t = 0) = 0$, showing the typical epidemic stages. The blue dashed line corresponds to $n/n_{\text{crit}} = 1$. (c) Schematic of Rydberg atoms (red dots) spanning facilitation shells (yellow region) and blockade spheres (red region). Ground-state atoms (gray dots) in the blue region are subject to off-resonant laser coupling. (d) Schematic phase diagram for the high (top) and low (bottom) temperature regimes depending on the total gas density n.

mixing limit for a gas of high temperatures [34]. The latter corresponding to an annealed random network.

For Rydberg facilitation systems, each atom can be considered as a three-level system with the ground (susceptible), Rydberg (infected), and inert or ionized (recovered) states [see Fig. 1(a)]. A concrete mapping of the Rydberg facilitation system to SIS and SIR models will be discussed later. The decay from the Rydberg to the inert state, given by the rate $b\gamma$, results in a loss of susceptible and infected individuals in the population, moving the system into an absorbing state. This gives rise to three typical epidemic stages, which were experimentally observed in Rydberg facilitation systems [20]. Following an initial infection, there is a rapid epidemic growth in infected individuals, or Rydberg atoms, in the system. This is followed by a saturation and an eventual relaxation at long times as a result of the system reaching an absorbing-state on these timescales [see Fig. 1(b)].

To describe the macroscopic dynamics of the Rydberg facilitation process in a gas, a simple mean-field model was put forward in [18], which, however, fails to provide a quantitative prediction of the microscopic dynamics, accurately calculated by Monte Carlo simulations [34] (see Fig. 2). This discrepancy results from the mean-field model not regarding (i) Rydberg blockade, which prevents the excitation of any atom closer than some radius r_{blockade} to a Rydberg atom and (ii) the emergent ER network at low temperatures.

In the following, we will develop a mean-field description of the dynamics of Rydberg excitations in a many-body-facilitated gas that accounts for both of these effects and provides accurate predictions of the full facilitation dynamics, which we demonstrate by comparing our predictions with
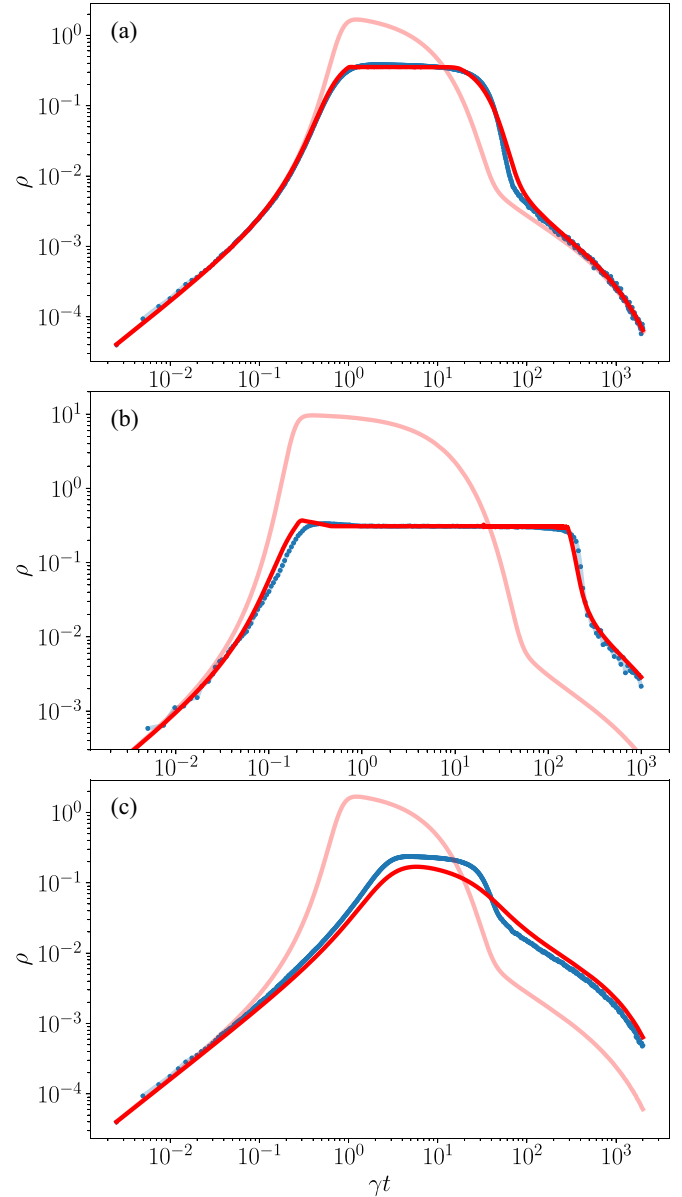
FIG. 2. Rydberg density ρ over time for $\rho(t = 0) = 0$ and $b = 0.3$ modeled with Monte Carlo simulations (blue dots), Eq. (12) (red, faint), and Eq. (33) (red, solid), for (a) high-temperature gas with starting density $n_0 = 4.0\, r_{\text{f}}^{-3} > n_{\text{crit}}$, (b) low-temperature percolating gas with $n_0 = 20\, r_{\text{f}}^{-3} > n_{\text{perc}}$, and (c) low-temperature nonpercolating gas with $n_0 = 4\, r_{\text{f}}^{-3} < n_{\text{perc}}$.

Monte Carlo simulations. The network structure of the cold gas leads to a higher total gas density at very long times and subsequently a higher Rydberg density in the saturation phase in comparison to mean-field predictions. Rydberg blockade causes a significant modification of the facilitation (infection) rate if the density of Rydberg excited atoms (infected individuals) reaches some threshold value. Similarly to the effect of regulatory measures on the dynamics of epidemics ("lockdown"), it limits the maximum density of Rydberg-excited atoms (infected individuals), but at the same time leads to a substantial prolongation of the slow transition into the absorbing (recovery) phase.

II. MICROSCOPIC MODEL OF RYDBERG FACILITATION

A microscopic description of Rydberg facilitation in a gas can be achieved from a Lindblad master equation of the density matrix $\hat{\rho}$ which takes the form

$$\frac{\mathrm{d}}{\mathrm{d}t}\hat{\rho} = i[\hat{\rho}, \hat{\mathcal{H}}] + \sum_l \hat{L}_l \hat{\rho} \hat{L}_l^\dagger - \frac{1}{2}\{\hat{L}_l^\dagger \hat{L}_l, \hat{\rho}\}, \qquad (4)$$

with the atom-light interaction Hamiltonian $\hat{\mathcal{H}}$ given by

$$\hat{\mathcal{H}} = \sum_i \left[\Omega(\hat{\sigma}_i^{gr} + \hat{\sigma}_i^{rg}) + \left(\sum_{j\neq i} \frac{c_6}{r_{ij}^6}\hat{\sigma}_j^{rr} - \Delta \right)\hat{\sigma}_i^{rr} \right]. \quad (5)$$

Here $\hat{\sigma}_i^{\mu\nu} = |\mu\rangle_{ii}\langle\nu|$ is the projection operator of the ith atom from the internal state ν to μ. The external driving field is described by the Rabi frequency Ω and the detuning Δ, and the van der Waals interaction energy between Rydberg atoms i and j is given by c_6/r_{ij}^6, with r_{ij} being the distance between the atoms. Finally, in Eq. (4) dissipation is described by the jump operators $\hat{L}_l$. These take the form $\hat{L}_1^{(i)} = \sqrt{(1-b)\gamma}\hat{\sigma}_i^{gr}$, $\hat{L}_2^{(i)} = \sqrt{b\gamma}\hat{\sigma}_i^{0r}$ for spontaneous decay from $|r\rangle$ to $|g\rangle$ and $|0\rangle$, as well as $\hat{L}_3^{(i)} = \sqrt{\gamma_\perp}\hat{\sigma}_i^{rr}$ for the dephasing of the Rydberg state. The parameter $b \in [0, 1]$ corresponds to the percentage of Rydberg atoms, which spontaneously decay to $|0\rangle$ and are thereby removed from the system. Therefore, if $b = 0$ the system corresponds to a two-level system and resembles an SIS epidemic [see Fig. 1(a)].

Dephasing results from, e.g., Doppler broadening or the spread of the atomic wave packet over the van der Waals potential [18,35]. In the large dephasing limit, the dynamics of a many-body Rydberg gas are effectively governed by classical rate equations [36]. As a result, this system can be simulated to great accuracy using Monte Carlo simulations. Starting from Eq. (4), after adiabatic elimination of coherences, one can formulate a set of rate equations for the probabilities of atom i being in the Rydberg state with $P_r^{(i)}$ or ground state with $P_g^{(i)}$ as

$$\frac{\mathrm{d}}{\mathrm{d}t}P_r^{(i)} = \Gamma_f(\Sigma)P_g^{(i)} - (\Gamma_f(\Sigma) + \gamma)P_r^{(i)}, \qquad (6a)$$

$$\frac{\mathrm{d}}{\mathrm{d}t}P_g^{(i)} = (\Gamma_f(\Sigma) + (1-b)\gamma)P_r^{(i)} - \Gamma_f(\Sigma)P_g^{(i)}, \quad (6b)$$

with the stimulated excitation rate given by

$$\Gamma_f(\Sigma) = \frac{2\Omega^2\gamma_\perp}{\gamma_\perp^2 + \Delta^2 \left(\sum_{\substack{j\neq i \\ j\in\Sigma}} \frac{r_f^6}{r_{ij}^6} - 1\right)^2}. \qquad (7)$$

Here Σ is the set of indices of Rydberg-excited atoms. If no other Rydberg atom exists in the gas or their distance is much larger than r_f, $\Gamma_f(\Sigma)$ reduces to the off-resonant excitation rate of an isolated atom

$$\tau = \frac{2\Omega^2\gamma_\perp}{\gamma_\perp^2 + \Delta^2}. \qquad (8)$$

If a Rydberg atom is present in the system, the atoms located around a certain distance to it, called facilitation distance r_f, are shifted into resonance and can be excited on a much faster timescale, given by the facilitation rate $\Gamma_f = 2\Omega^2/\gamma_\perp$. The

facilitation distance is given by

$$r_f = \sqrt[6]{\frac{c_6}{\Delta}}. \qquad (9)$$

Rydberg facilitation can be observed when $\Delta \gg \Omega$, as this naturally gives rise to a hierarchy in timescales such that

$$\Gamma_f \gg \gamma \gg \tau. \qquad (10)$$

In this case, off-resonant excitations and the decay of Rydberg atoms are effectively static on the timescale of facilitated excitations. Each Rydberg atom spans a spherical shell, with distance r_f and approximate width δr_f, in which atoms are resonantly coupled to the driving laser field. The width of the facilitation shell is thereby determined by the effective linewidth of the excitation transition and reads

$$\delta r_f = \frac{\gamma_\perp}{2\Delta}r_f. \qquad (11)$$

Atoms closer than $r_f - \delta r_f/2$ to a Rydberg atom are subject to Rydberg blockade [3] and cannot be excited since they are shifted out of resonance again. These three regions around a Rydberg atom (off-resonant coupling, facilitation, and blockade) can be schematically seen in Fig. 1(c).

In [18], a mean-field equation for a macroscopic description of the many-body Rydberg facilitation dynamics has been derived. For a homogeneous gas this reads

$$\frac{\mathrm{d}}{\mathrm{d}t}\rho = -\kappa(2\rho^2 - \rho n) - \gamma\rho - \tau(2\rho - n), \qquad (12a)$$

$$\frac{\mathrm{d}}{\mathrm{d}t}n = -b\gamma\rho. \qquad (12b)$$

Here ρ corresponds to the coarse-grained Rydberg density (in a small volume ΔV)

$$\rho(\vec{r}, t) = \frac{1}{\Delta V} \sum_{i:\vec{r}_i\in\Delta V} \langle\hat{\sigma}_i^{rr}\rangle, \qquad (13)$$

and n is the density of ground and Rydberg state atoms

$$n(\vec{r}, t) = \frac{1}{\Delta V} \sum_{i:\vec{r}_i\in\Delta V} \left(\langle\hat{\sigma}_i^{rr}\rangle + \langle\hat{\sigma}_i^{gg}\rangle\right). \qquad (14)$$

Note that n does not count $|0\rangle$ state atoms and therefore decreases over time if $b > 0$. The spreading rate of Rydberg excitations in the many-body gas is given by the two-body facilitation rate integrated over the facilitation shell

$$\kappa = \Gamma_f V_s, \qquad (15)$$

with the volume of the facilitation shell $V_s \approx 4\pi \delta r_f r_f^2$. The above equations predict an absorbing-state phase transition between an active and absorbing phase for the critical gas density

$$n_{\mathrm{crit}} = \frac{\gamma}{\Gamma_f V_s}. \qquad (16)$$

Equation (12a) for the (mean-field) Rydberg density in the many-body gas strongly resembles the SIS equation of motion of infected individuals given by Eq. (1a). However, in contrast to SIS-SIR epidemics, Rydberg systems additionally feature (i) off-resonant excitations with rate τ, (ii) resonant (facilitated) *de*excitations of Rydberg atoms [described by the

term $-2\kappa\rho^2$ in Eq. (12a)], and (iii) Rydberg blockade which is not regarded in Eq. (12a).

For the atom number conserving limit ($b = \tau = 0$) [18], Eq. (12a) directly maps to those of the SIS dynamics [Eq. (1)] by identifying $\rho^I = 2\rho$ and $\rho^S = n - 2\rho \geqslant 0$ with conserved total density $\rho^I + \rho^S = n - 2\rho + 2\rho = n$. Moreover in the high-temperature limit, the deexcitation can effectively be neglected as it is a second-order process in terms of Rydberg density.

For the low-temperature gas, the excitation dynamics are constrained to an ER network in which the individual nodes are comprised of atoms (either in $|g\rangle$ or $|r\rangle$), and connections between nodes, say i and j, exist if $r_{ij} \approx r_f$. The number of connections a node has (i.e., the number of atoms with distance r_f to an atom) is called the degree k of the atom. In an ER network the node degrees follow a Poissonian distribution with average degree

$$\langle k \rangle = n V_s. \tag{17}$$

An ER network features a percolation transition at $\langle k \rangle = 1$ between an (almost fully) connected network and a fragmented network, comprised of many small disconnected clusters. Here, clusters refers to a group of connected nodes. From Eq. (17), we can identify the gas density at which the percolation transition occurs as

$$n_{\text{perc}} = \frac{1}{V_s}. \tag{18}$$

This density is a factor Γ_f/γ larger than the critical density of the phase transition to the absorbing phase for a homogeneous gas [34]. A schematic phase diagram for the high- and low-temperature gas can be seen in Fig. 1(d). For further details on the mapping of the Rydberg facilitation gas to an ER network see [34].

In this paper, we model the actual many-body dynamics using Monte Carlo simulations of the rate equations (6). We assume a cubic box with length $L = 7r_f$ and periodic boundary conditions. Atom positions are chosen randomly and velocities are sampled from a Maxwell-Boltzmann distribution with temperature parameter $\hat{v}$, corresponding to the most probable atom velocity in the gas. For the time evolution we utilize a fixed time step Monte Carlo algorithm [37], with the time step $dt = 1/400\,\gamma^{-1}$, as long-range interactions paired with the fast movement of atoms in the high-temperature case results in quickly changing transitional rates in the system. To ensure numeric stability the c_6 potential in Eq. (7) is truncated at a cutoff value around the singularity $r_{ij} \to 0$.

III. MODIFIED LANGEVIN DESCRIPTION OF EPIDEMIC EVOLUTION

In the following section, we develop an effective macroscopic theory of the Rydberg facilitation process, expanding the Langevin equation (12), starting from the microscopic model. This new equation takes into account Rydberg blockade, as well as the network structure in the case of the low-temperature gas.

In Fig. 2, the dynamics of Rydberg excitations predicted by the improved Langevin equation and by Monte Carlo simulations are compared for the cases: (i) high-temperature gas with

$n_0 > n_{\text{crit}}$, (ii) low-temperature gas initially above the percolation threshold with $n_0 > n_{\text{perc}}$, and (iii) low-temperature gas initially below the percolation threshold $n_0 < n_{\text{perc}}$. Here n_0 refers to the gas density at $t = 0$. Additionally, we use a branching parameter $b = 0.3$, allowing some loss into the recovered state $|0\rangle$. Therefore, for all cases (i) to (iii), the system drives itself to the absorbing-state and follows the typical epidemic stages as seen in Fig. 1(b).

We start from the microscopic Heisenberg-Langevin equations describing the quantum many-body dynamics of Rydberg excitations for atoms at given spatial positions given by

$$\frac{d}{dt}\hat{\sigma}_i^{rr} = -i\Omega(\hat{\sigma}_i^{rg} - \hat{\sigma}_i^{gr}) - \gamma\hat{\sigma}_i^{rr} + \hat{\xi}_1, \tag{19}$$

$$\frac{d}{dt}\hat{\sigma}_i^{rg} = -i(\Omega(\hat{\sigma}_i^{rr} - \hat{\sigma}_i^{gg}) - \hat{V}_i\hat{\sigma}_i^{rg}) - \gamma_\perp\hat{\sigma}_i^{rg} + \hat{\xi}_2. \tag{20}$$

These equations can be obtained from the Lindblad master equation [Eq. (4)] using $\frac{d}{dt}\langle\hat{\sigma}_i^{rr}\rangle = \text{Tr}\{\hat{\sigma}_i^{rr}\frac{d}{dt}\hat{\rho}\}$ noting that for the operator dynamics a Langevin noise term $\hat{\xi}$ has to be added to conserve commutation relations [38]. These noise terms disappear in the quantum mechanical average and their properties can be obtained from the fluctuation-dissipation relation [39].

The operator $\hat{V}_i$ describes the detuning of the ith atom and depends on the states of all other atoms. It is given by

$$\hat{V}_i = \Delta\left(-1 + \sum_{j\neq i}\frac{r_f^6}{r_{ij}^6}\hat{\sigma}_j^{rr}\right). \tag{21}$$

We note that the operator-valued quantities are objects in Hilbert space describing the quantum mechanical evolution and are subject to the classical statistics of the (time-dependent) random positions of the atoms. The dynamics of the atom positions are treated classically, which is well justified in the high-dephasing limit, assumed throughout the present paper.

Furthermore, the effect of c_6 forces acting on the center-of-mass motion of the atoms due to the distance dependence of $\hat{V}_i$ are disregarded in the present paper. They will be discussed elsewhere in more detail [40], where we will show that, under typical experimental conditions, they can be accounted for by a change of the atoms velocity distribution and, in the case of a trapped gas, by an additional loss channel.

Assuming high dephasing $\gamma_\perp \geqslant \Omega$, the coherences $\hat{\sigma}_i^{rg}$ quickly decay to quasistationary values relative to the relevant many-body timescales. Therefore, we adiabatically eliminate coherences ($\frac{d}{dt}\hat{\sigma}_i^{rg} = 0$) and arrive at

$$\frac{d}{dt}\hat{\sigma}_i^{rr} = -\frac{2\Omega^2\gamma_\perp}{\gamma_\perp^2 + \hat{V}_i^2}(\hat{\sigma}_i^{rr} - \hat{\sigma}_i^{gg}) - \gamma\hat{\sigma}_i^{rr} + \hat{\xi}. \tag{22}$$

As a result of the quickly decaying potential $\hat{V}_i$ with interatomic distance, only Rydberg atoms with distances $r_{ij} \leqslant r_f$ are relevant for the internal dynamics of atom i. Therefore, we can perform a spatially local approximation by introducing the projection operator $\hat{\Pi}_i(m)$, projecting onto m Rydberg atoms with distances $r_{ij} \leqslant r_f$. Using the completeness relation

$$\sum_m \hat{\Pi}_i(m) = \hat{\mathbb{1}}, \tag{23}$$

we are able to expand the fraction in Eq. (22) giving

$$
\begin{aligned}
\frac{\mathrm{d}}{\mathrm{d}t}\hat{\sigma}_i^{rr} = {} & -\hat{\Pi}_i(0)\frac{2\Omega^2\gamma_\perp}{\gamma_\perp^2+\Delta^2}\big(\hat{\sigma}_i^{rr}-\hat{\sigma}_i^{gg}\big) \\
& -\hat{\Pi}_i(1)\underbrace{\frac{2\Omega^2\gamma_\perp}{\gamma_\perp^2+\Delta^2\big(\big(\frac{r_\mathrm{f}}{r_{1i}}\big)^6-1\big)^2}}_{(*)}\big(\hat{\sigma}_i^{rr}-\hat{\sigma}_i^{gg}\big) \\
& +\cdots \\
& -\gamma\hat{\sigma}_i^{rr}+\hat{\xi}.
\end{aligned}
\tag{24}
$$

All rates for more than one Rydberg atom in the facilitation *sphere* ($m>1$) are strongly suppressed due to blockade. As a result, we truncate the expansion at $m=1$.

Finally, we calculate the expectation value of the operator $\hat{\sigma}_i^{rr}$ with a double averaging over the quantum mechanical state and the ensemble of the many different atom positions in the gas. We will denote these double averages as $\langle\langle\hat{\sigma}_i^{rr}\rangle\rangle$ and write

$$
\begin{aligned}
\frac{\mathrm{d}}{\mathrm{d}t}\langle\langle\hat{\sigma}_i^{rr}\rangle\rangle = {} & -\tau\big\langle\!\big\langle\hat{\Pi}_i(0)\big(\hat{\sigma}_i^{rr}-\hat{\sigma}_i^{gg}\big)\big\rangle\!\big\rangle \\
& -\Gamma_\mathrm{f}\big\langle\!\big\langle\hat{\Pi}_i(1)\big(\hat{\sigma}_i^{rr}-\hat{\sigma}_i^{gg}\big)\big\rangle\!\big\rangle \\
& -\gamma\big\langle\!\big\langle\hat{\sigma}_i^{rr}\big\rangle\!\big\rangle \\
\approx {} & -\tau\langle\langle\hat{\Pi}_i(0)\rangle\rangle\big(\langle\langle\hat{\sigma}_i^{rr}\rangle\rangle-\langle\langle\hat{\sigma}_i^{gg}\rangle\rangle\big) \\
& -\Gamma_\mathrm{f}\,p_\mathrm{shell}\langle\langle\hat{\Pi}_i(1)\rangle\rangle\big(\langle\langle\hat{\sigma}_i^{rr}\rangle\rangle-\langle\langle\hat{\sigma}_i^{gg}\rangle\rangle\big) \\
& -\gamma\langle\langle\hat{\sigma}_i^{rr}\rangle\rangle.
\end{aligned}
\tag{25,26}
$$

Here we introduce the off-resonant excitation rate $\tau=\frac{2\Omega^2\gamma_\perp}{\gamma_\perp^2+\Delta^2}$, the facilitated excitation rate $\Gamma_\mathrm{f}=\frac{2\Omega^2}{\gamma_\perp}$, and (assuming a randomly distributed gas) the classical probability $p_\mathrm{shell}=V_s/V_f$ that the Rydberg atom is in the facilitation *shell* if it is already in the facilitation *sphere*.

With the random gas assumption, we can approximate the probabilities $\langle\langle\hat{\Pi}_i(m)\rangle\rangle$ as Poissonian with the rate ρV_f (i.e., $\langle\langle\hat{\Pi}_i(m)\rangle\rangle=(\rho V_f)^m e^{-\rho V_f}/m!$) resulting in

$$
\langle\langle\hat{\Pi}_i(0)\rangle\rangle = e^{-\rho V_\mathrm{f}},
\tag{27}
$$

$$
p_\mathrm{shell}\langle\langle\hat{\Pi}_i(1)\rangle\rangle \equiv \frac{V_s}{V_f}\langle\langle\Pi_i(1)\rangle\rangle = \rho V_s\,e^{-\rho V_\mathrm{f}}.
\tag{28}
$$

We then perform the coarse-graining given by Eqs. (13) and (14) and arrive at

$$
\begin{aligned}
\frac{\mathrm{d}}{\mathrm{d}t}\rho = {} & -\kappa e^{-\rho V_\mathrm{f}}\rho(2\rho-n) \\
& -\gamma\rho-\tau(2\rho-n).
\end{aligned}
\tag{29}
$$

Furthermore, we assume here $e^{-\rho V_\mathrm{f}}\tau\approx\tau$ as the off-resonant rate is only relevant when $\rho V_\mathrm{f}\ll1$.

The spreading rate of excitations κ is now exponentially damped by the density of Rydberg atoms. This gives a better description of the spreading of Rydberg excitations in the epidemic growth stage. However, as all atoms with distances closer than r_blockade to a Rydberg atom cannot be excited due to Rydberg blockade [red region in Fig. 1(c)], there exists a maximum density of Rydberg atoms ρ_max, given by the

packing density of nonoverlapping spheres, above which no more excitations are possible.

To quantify the blockade induced saturation density in the gas, we introduce the parameter η corresponding to the packing density of spheres in a given volume.

For the high-temperature gas, this corresponds to the densest packing of spheres, given by $\eta=\frac{\pi}{3\sqrt{2}}\approx74.0\%$. In this regime we can assume this packing density to be achieved, as the high motion of the atoms allow the system to organize itself to this state.

For the frozen gas, the packing density is slightly lower, and is given by the closest density of *randomly* packed spheres, which is given by $\eta\approx63.5\%$ [41].

As $\delta r_\mathrm{f}\ll r_\mathrm{f}$ we can approximate the blockade radius as $r_\mathrm{blockade}\approx r_\mathrm{f}$ and write

$$
\rho_\mathrm{max}=2\frac{\eta}{V_\mathrm{fac}},
\tag{30}
$$

with the approximate volume of the blockade sphere $V_\mathrm{fac}=\frac{4}{3}\pi r_\mathrm{f}^3$. The factor of 2 emerges as when a facilitation event occurs, the facilitated atom is centered on the blockade sphere of the facilitating Rydberg atom. As a result, the blockade spheres of these atoms overlap. If, however, a third Rydberg atom is facilitated (by the second Rydberg atom), its blockade sphere borders the blockade sphere of the first Rydberg atom with, on average, very little overlap [see Fig. 1(c)].

As the laser coupling smoothly changes from resonant, for an atom with distance $r=r_\mathrm{f}$ to a Rydberg atom, to strongly suppressed for $r<r_\mathrm{f}$, this can be regarded as a packing of soft spheres with an uncertainty in volume of $\delta V_\mathrm{fac}=4\pi\,\delta r_\mathrm{f}r_\mathrm{f}^2$. The result is a smearing out of ρ_max given by $\delta\rho_\mathrm{max}=\delta V_\mathrm{fac}\frac{2\eta}{V_\mathrm{fac}^2}$. We can now add a heuristic function which sets the facilitation rate to 0 if $\rho>\rho_\mathrm{max}$ as

$$
h(\rho)=\frac{1}{2}\left[1+\tanh\left(\frac{\rho_\mathrm{max}-\rho}{\delta\rho_\mathrm{max}}\right)\right].
\tag{31}
$$

The added factors $e^{-\rho V_\mathrm{f}}$ and $h(\rho)$ to the facilitation rate κ suffice to accurately describe the dynamics of the Rydberg density in the high-temperature gas [see Fig. 2(a)].

Moreover, the truncation of the maximum number of infected individuals as a result of blockade gives qualitative agreement with the effect of control measures such as lockdowns seen in the COVID-19 pandemic [42].

For the low-temperature gas the finite connectivity greatly reduces the facilitation rate. Taking into account that facilitation can only occur if the degree of the atom k is not 0, we alter the facilitation rate to

$$
\kappa\to\kappa\,P(k>0).
\tag{32}
$$

For an ER network with average degree $\langle k\rangle\ll1$, we can approximate $P(k>0)\approx\langle k\rangle$. In this case the new infection rate κ corresponds to the Kephart-White model [43,44].

The full Langevin equation for the Rydberg density reads

$$
\begin{aligned}
\frac{\mathrm{d}}{\mathrm{d}t}\rho = {} & -\kappa e^{-\rho V_\mathrm{f}}h(\rho)P(k>0)\rho(2\rho-n) \\
& -\gamma\rho-\tau(2\rho-n),
\end{aligned}
\tag{33}
$$

with $P(k > 0) = 1 - e^{-nV_s}$ for the low-temperature gas and $P(k > 0) = 1$ at high temperatures, as the thermal velocity of atoms allows for random-mixing of all atoms. As a result, the high-temperature regime is described excellently by the classical SIS-SIR models [Eqs. (1) and (3)] with the addition of blockade.

In Fig. 2 we compare the predictions from the modified Langevin equation (33) with Monte Carlo simulations in the high-temperature gas, the frozen percolating gas, and the frozen nonpercolating gas. For the high temperature and the frozen percolating case, Eq. (33) has a very good agreement for all epidemic stages with Monte Carlo data. In particular, it predicts the correct density in the saturation stage in the high-temperature and the low-temperature percolating gas in contrast to Eq. (12).

Furthermore, for the case of the low temperature gas, Eq. (33) gives a much better approximation of the relaxation epidemic stage (i.e., for times $\gamma t \gtrsim 10^2$). In this stage, the Rydberg density is much higher than the expected MF density (predicted by the faint red line), which holds for high temperatures. In contrast to the high-temperature regime, the system leaves the active phase at much higher gas density due to the finite connectivity of excitation paths in the gas. The factor $P(k > 0)$ in the facilitation rate gives a much better approximation of this increased Rydberg density.

IV. CONCLUSION

In conclusion, we developed a modified mean-field approach to model the Rydberg density over time in a many-body gas under facilitation conditions for the limits of high and low temperature. In the low temperature regime, we additionally differentiated between a system with initial density $n_0 > n_{\mathrm{prec}}$ and $n_0 < n_{\mathrm{perc}}$, where n_{perc} is the percolation density below which heterogeneous effects play a large role.

Our modeling is similar to that developed in [18], but with three key improvements to the facilitation (or infection) rate κ. We consider (i) random atom positions leading to a Poissonian distribution in the number of Rydberg atoms closer than r_{blockade} to a given atom. In this case, the atom cannot be excited or deexcited due to Rydberg blockade. As a result,

with increasing Rydberg density, the global facilitation rate κ exponentially decreases.

Additionally, (ii) excited Rydberg atoms can be seen as soft spheres inside of which no atoms can be excited due to blockade. Therefore, there exists a tightest packing of excited atoms beyond which the facilitation rate κ vanishes. In the high-temperature regime, this packing density corresponds to the tightest packing of spheres in a given volume, as the high thermal velocities allow the system to continuously organize itself to this state. In the low-temperature regime the packing density is given by that of randomly placed spheres in a given volume, which, in comparison, is slightly lower.

Finally, (iii) for the low-temperature regime, one has to additionally consider the finite connectivity of the underlying network along which facilitated excitations can spread. On a mean-field level, we described this by reducing the facilitation rate in correspondence with the portion of atoms with network degree (i.e., the number of atoms in their facilitation shell) $k = 0$. The percentage of these isolated atoms increases as the network connectivity decreases, and is therefore dependent on the total density of the gas.

For both the high temperature, as well as the low temperature, high density case Eq. (33) gives excellent correspondence to Monte Carlo data for all epidemic stages.

For the low temperature, low density gas the system is characterized by strong heterogeneity making an accurate mean-field description challenging. However, for this case we still see a large improvement in the Langevin description of the dynamics.

[1] T. Gallagher, *Rydberg Atoms* (Springer, New York, 2006).

[2] D. Jaksch, J. I. Cirac, P. Zoller, S. L. Rolston, R. Côté, and M. D. Lukin, Fast quantum gates for neutral atoms, Phys. Rev. Lett. **85**, 2208 (2000).

[3] M. D. Lukin, M. Fleischhauer, R. Cote, L. M. Duan, D. Jaksch, J. I. Cirac, and P. Zoller, Dipole blockade and quantum information processing in mesoscopic atomic ensembles, Phys. Rev. Lett. **87**, 037901 (2001).

[4] A. Gaetan, Y. Miroshnychenko, T. Wilk, A. Chotia, M. Viteau, D. Comparat, P. Pillet, A. Browaeys, and P. Grangier, Observation of collective excitation of two individual atoms in the Rydberg blockade regime, Nat. Phys. **5**, 115 (2009).

[5] E. Urban, T. A. Johnson, T. Henage, L. Isenhower, D. Yavuz, T. Walker, and M. Saffman, Observation of Rydberg blockade between two atoms, Nat. Phys. **5**, 110 (2009).

[6] M. Saffman, T. G. Walker, and K. Mølmer, Quantum information with Rydberg atoms, Rev. Mod. Phys. **82**, 2313 (2010).

[7] H. Weimer, M. Müller, I. Lesanovsky, P. Zoller, and H. P. Büchler, A Rydberg quantum simulator, Nat. Phys. **6**, 382 (2010).

[8] P. Schauß, M. Cheneau, M. Endres, T. Fukuhara, S. Hild, A. Omran, T. Pohl, C. Gross, S. Kuhr, and I. Bloch, Observation of spatially ordered structures in a two-dimensional Rydberg gas, Nature (London) **491**, 87 (2012).

[9] H. Bernien, S. Schwartz, A. Keesling, H. Levine, A. Omran, H. Pichler, S. Choi, A. S. Zibrov, M. Endres, M. Greiner, V. Vuletić, and M. D. Lukin, Probing many-body dynamics on a 51-atom quantum simulator, Nature (London) **551**, 579 (2017).

[10] A. Browaeys and T. Lahaye, Many-body physics with individually controlled Rydberg atoms, Nat. Phys. **16**, 132 (2020).

[11] F. M. Surace, P. P. Mazza, G. Giudici, A. Lerose, A. Gambassi, and M. Dalmonte, Lattice gauge theories and string dynamics in Rydberg atom quantum simulators, Phys. Rev. X **10**, 021041 (2020).

[12] P. Scholl, M. Schuler, H. J. Williams, A. A. Eberharter, D. Barredo, K.-N. Schymik, V. Lienhard, L.-P. Henry, T. C. Lang, T. Lahaye, A. M. Läuchli, and A. Browaeys, Quantum simulation of 2D antiferromagnets with hundreds of Rydberg atoms, Nature (London) **595**, 233 (2021).

[13] S. de Léséleuc, V. Lienhard, P. Scholl, D. Barredo, S. Weber, N. Lang, H. P. Büchler, T. Lahaye, and A. Browaeys, Observation of a symmetry-protected topological phase of interacting bosons with Rydberg atoms, Science **365**, 775 (2019).

[14] G. Semeghini, H. Levine, A. Keesling, S. Ebadi, T. T. Wang, D. Bluvstein, R. Verresen, H. Pichler, M. Kalinowski, R. Samajdar, A. Omran, S. Sachdev, A. Vishwanath, M. Greiner, V. Vuletić, and M. D. Lukin, Probing topological spin liquids on a programmable quantum simulator, Science **374**, 1242 (2021).

[15] S. Helmrich, A. Arias, and S. Whitlock, Uncovering the nonequilibrium phase structure of an open quantum spin system, Phys. Rev. A **98**, 022109 (2018).

[16] M. Magoni, P. Mazza, and I. Lesanovsky, Phonon dressing of a facilitated one-dimensional Rydberg lattice gas, SciPost Physics Core **5**, 041 (2022).

[17] M. Marcuzzi, J. Minář, D. Barredo, S. de Léséleuc, H. Labuhn, T. Lahaye, A. Browaeys, E. Levi, and I. Lesanovsky, Facilitation dynamics and localization phenomena in Rydberg lattice gases with position disorder, Phys. Rev. Lett. **118**, 063606 (2017).

[18] S. Helmrich, A. Arias, G. Lochead, T. M. Wintermantel, M. Buchhold, S. Diehl, and S. Whitlock, Signatures of self-organized criticality in an ultracold atomic gas, Nature (London) **577**, 481 (2020).

[19] D.-S. Ding, H. Busche, B.-S. Shi, G.-C. Guo, and C. S. Adams, Phase diagram and self-organizing dynamics in a thermal ensemble of strongly interacting Rydberg atoms, Phys. Rev. X **10**, 021023 (2020).

[20] T. M. Wintermantel, M. Buchhold, S. Shevate, M. Morgado, Y. Wang, G. Lochead, S. Diehl, and S. Whitlock, Epidemic growth and griffiths effects on an emergent network of excited atoms, Nat. Commun. **12**, 103 (2021).

[21] R. M. Anderson and R. M. May, *Infectious Diseases of Humans: Dynamics and Control* (Oxford University Press, New York, 1991).

[22] N. T. Bailey *et al.*, *The Mathematical Theory of Infectious Diseases and its Applications* (Charles Griffin & Company, High Wycombe, England, 1975).

[23] J. D. Murray, Epidemic models and the dynamics of infectious diseases, Math. Biol. **19**, 610 (1993).

[24] R. Pastor-Satorras, C. Castellano, P. Van Mieghem, and A. Vespignani, Epidemic processes in complex networks, Rev. Mod. Phys. **87**, 925 (2015).

[25] M. J. Keeling and K. T. Eames, Networks and epidemic models, J. R. Soc., Interface **2**, 295 (2005).

[26] T. Harko, F. S. Lobo, and M. Mak, Exact analytical solutions of the susceptible-infected-recovered (sir) epidemic model and

[27] of the sir model with equal death and birth rates, Appl. Math. Comput. **236**, 184 (2014).

[27] O. N. Bjørnstad, K. Shea, M. Krzywinski, and N. Altman, Modeling infectious epidemics, Nature Methods **17**, 455 (2020).

[28] R. Beckley, C. Weatherspoon, M. Alexander, M. Chandler, A. Johnson, and G. S. Bhatt, Modeling epidemics with differential equations, Tennessee State University Internal Report, 2013.

[29] P. Erdős and A. Rényi, On the evolution of random graphs, Publ. Math. Inst. Hung. Acad. Sci **5**, 17 (1960).

[30] A.-L. Barabási, Scale-free networks: a decade and beyond, Science **325**, 412 (2009).

[31] R. Pastor-Satorras and A. Vespignani, Epidemic spreading in scale-free networks, Phys. Rev. Lett. **86**, 3200 (2001).

[32] R. Pastor-Satorras and A. Vespignani, Epidemic dynamics in finite size scale-free networks, Phys. Rev. E **65**, 035108(R) (2002).

[33] C. Durón and A. Farrell, A mean-field approximation of sir epidemics on an erdös–rényi network model, Bull. Math. Biol. **84**, 70 (2022).

[34] D. Brady, J. Bender, P. Mischke, T. Niederprüm, H. Ott, and M. Fleischhauer, Griffiths phase in a facilitated Rydberg gas at low temperature, arXiv:2302.14145.

[35] W. Li, C. Ates, and I. Lesanovsky, Nonadiabatic motional effects and dissipative blockade for Rydberg atoms excited from optical lattices or microtraps, Phys. Rev. Lett. **110**, 213005 (2013).

[36] E. Levi, R. Gutiérrez, and I. Lesanovsky, Quantum nonequilibrium dynamics of Rydberg gases in the presence of dephasing noise of different strengths, J. Phys. B: At., Mol. Opt. Phys. **49**, 184003 (2016).

[37] V. Ruiz Barlett, J. Bigeón, M. Hoyuelos, and H. Mártin, Differences between fixed time step and kinetic monte carlo methods for biased diffusion, J. Comput. Phys. **228**, 5740 (2009).

[38] C. Gardiner and P. Zoller, *Quantum Noise: A Handbook of Markovian and Non-Markovian Quantum Stochastic Methods with Applications to Quantum Optics* (Springer Science & Business Media, New York, 2004).

[39] R. Kubo, The fluctuation-dissipation theorem, Rep. Prog. Phys. **29**, 255 (1966).

[40] D. Brady and M. Fleischhauer, (unpublished).

[41] Y. Wu, Z. Fan, and Y. Lu, Bulk and interior packing densities of random close packing of hard spheres, J. Mater. Sci. **38**, 2019 (2003).

[42] T. Oraby, M. G. Tyshenko, J. C. Maldonado, K. Vatcheva, S. Elsaadany, W. Q. Alali, J. C. Longenecker, and M. Al-Zoughool, Modeling the effect of lockdown timing as a covid-19 control measure in countries with differing social contacts, Sci. Rep. **11**, 3354 (2021).

[43] J. O. Kephart and S. R. White, Directed-graph epidemiological models of computer viruses, in *Computation: The Micro and the Macro View* (World Scientific, Singapore, 1992), pp. 71–102.

[44] D. Chakrabarti, Y. Wang, C. Wang, J. Leskovec, and C. Faloutsos, Epidemic thresholds in real networks, ACM Transactions on Information and System Security (TISSEC) **10**, 1 (2008).